ELSEVIER

Available online at www.sciencedirect.com

SCIENCE DIRECT

Solar Energy Materials & Solar Cells 87 (2005) 795–805

Solar Energy Materials & Solar Cells

www.elsevier.com/locate/solmat

Plasma emission diagnostics for the transition from microcrystalline to amorphous silicon solar cells

E. Amanatides[a], D. Mataras[a,*], D. Rapakoulias[a], M.N. van den Donker[b], B. Rech[b]

[a]*Department of Chemical Engineering, Plasma Technology Laboratory, University of Patras, P.O. Box 1407, 26504 Patras, Greece*

[b]*Institute of Photovoltaics, Forschungszentrum Jülich GmbH, D-52425 Jülich, Germany*

Received 15 May 2004; received in revised form 30 June 2004; accepted 4 July 2004
Available online 25 November 2004

Abstract

The possibility to employ spatially resolved optical emission spectroscopy (SROES) as a diagnostic tool for the prediction of the transition from microcrystalline to amorphous silicon growth was investigated. The transition was achieved by increasing the silane fraction in the mixture and was identified through the solar cell performance. A drastic change of the shape of the emission profiles, characterized by an enhancement of the production of species closer to the substrate, was observed in the transition region when increasing the silane fraction. Calculations of the probability of various species to reach the surface have shown that the change of the shape of the radical generation distribution in space finally leads to an increase of the contribution of highly reactive, highly sticking radicals like SiH_2 to the film growth. On the other hand less reactive species like H atoms are less affected by the shape of their generation profiles. Their probability to reach the surface drops because of the increase of the collision frequency. Both these factors can explain the transition to amorphous silicon growth and the relation between emission profiles and the transition indicating a clear potential for using SROES in thin film solar cell performance optimization.
© 2004 Elsevier B.V. All rights reserved.

Keywords: Microcrystalline silicon; High pressure; Plasma emission spectroscopy

*Corresponding author. Tel.: +30 2610 997857; fax: +30 2610 993361.
E-mail addresses: dim@plasmatech.gr (D. Mataras), b.rech@fz-juelich.de (M.N. van den Donker).

0927-0248/$ - see front matter © 2004 Elsevier B.V. All rights reserved.
doi:10.1016/j.solmat.2004.07.052

1. Introduction

The use of hydrogenated microcrystalline silicon (μc-Si:H) in single- or multi-junction solar cells has shown an important potential for obtaining higher stable efficiencies [1]. Recent progress in understanding the properties of μc-Si:H absorbing layers has shown that higher cell efficiencies can be obtained when these films are deposited in the transition range between amorphous and microcrystalline growth [2]. The conditions leading to this transition depend on a combination of a number of plasma parameters as frequency, total pressure, gas flow, RF power and silane fraction. Thus, the optimization of the discharge conditions leading to the best suited films for application in solar cells is a time-consuming procedure requiring a large number of experiments. It would therefore be very useful to have a diagnostic tool able to predict this change thus allowing to fine tune the discharge conditions. Plasma emission has been suggested to serve as such a tool, based on the idea that the transition from the amorphous to the microcrystalline growth depends on changes in microscopic plasma properties [3].

In this work we present an investigation of the possibility of utilization of spatially resolved optical emission spectroscopy (SROES) for the prediction of the plasma conditions that lead to the growth of μc-Si:H films near the transition to amorphous silicon growth. For this purpose, depositions of intrinsic layers were carried out at two total gas pressures (5 and 10 Torr) and the transition from amorphous to microcrystalline growth was achieved by successively increasing the SiH_4 fraction in the gas mixture from 0.5 to 3.33%. At each condition, the spatial distribution of emission between the two electrodes from both the excited silylidine radical (SiH*, $A^2\Delta$) and the β-Balmer line of atomic hydrogen (H_β) were recorded with a spatial resolution of 1 mm.The spatial emission profiles thus obtained were compared with the characteristics of complete p–i–n cells deposited using the same apparatus and conditions. A relation was found between the transition and the emission profiles, as the successive increase of the SiH_4 fraction was found to modify the shape of the emission profiles indicating an enhanced production of species closer to the substrate in the amorphous regime. This correlation was further strengthened by calculating the effect of the change of the spatial distribution of species on their probability to reach the deposition surface. The results show that the enhanced production of species closer to the surface favours mainly the probability of species with high reactivity in the gas phase (SiH_2) to reach the surface, while the probability of other species with lower reactivity (H atoms) is less affected.

2. Experimental

Silicon thin films were prepared in a multi-chamber PECVD reactor with an electrode area of 150 cm^2 and interelectrode distance of 10 mm. The grounded electrode consists of a substrate holder suitable for $10 \times 10\,cm^2$ substrates, and the powered electrode is made in the showerhead configuration assuring a homogeneous gas supply. The thin film solar cells described in this paper are deposited in the p–i–n

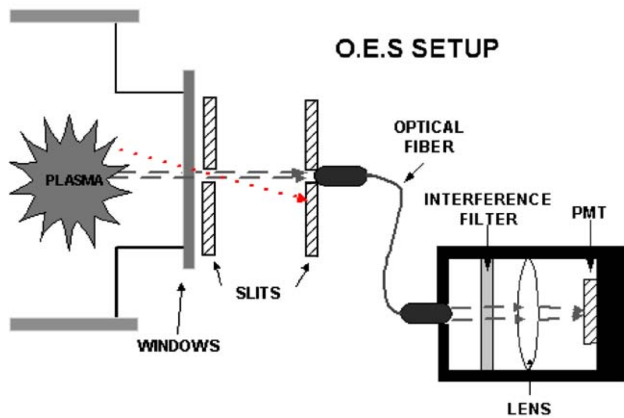

Fig. 1. Experimental setup used for recording spatially resolved emission profiles.

deposition sequence ('superstrate configuration') on texture-etched ZnO:Al coated glass substrates. The cell area, defined by a 500 nm Ag back contact, was 1 cm^2. Silicon layers in the cells were prepared using solely 13.56 MHz excitation frequency and the i-layers were deposited at 5 and 10 Torr and generator power of 80 W. The i-layer thickness and the corresponding deposition rate were determined by measuring the whole cell thickness with a step profiler and subtracting the thicknesses of the doped silicon layers (about 30 nm) and the ZnO.

The setup used for recording spatially resolved emission profiles is shown in Fig. 1. Light collection is made through an optical assembly comprising two slits, of 0.5 mm width and 2 cm height each and with a distance of 10 cm between them, located as close as possible to the reactor side optical window. An optical fibre, equipped with an entrance collimating lens set is directing the collected light through a suitable interference filter and a focusing lens to the entrance slit of a photomultiplier. The interference filters used were Ealing type 35-3250 and type 35-3458 for recording the emission intensity of the silylidine (SiH) radical and the β-Balmer line of atomic hydrogen, respectively. The slits assembly was mounted on an optical rail that is used for the linear translation of the system in parallel to the electrode axis in order to record complete spatial emission distribution profiles in the entire interelectrode space.

3. Results

Two set of experiments were performed in order to investigate the role of total gas pressure and of silane fraction in the gas mixture, on the transition from microcrystalline to amorphous silicon growth. The first one at the total gas pressure of 5 Torr and variable SiH_4 fraction from 0.5% to 3.33% and the second one at the gas pressure of 10 Torr and silane fraction from 0.5% to 2.2%. All other discharge parameters as nominal power, excitation frequency, total gas flow and electrode gap

were maintained constant at 80 Watt, 13.56 MHz, 360 sccm and 10 mm, respectively. Spatially Resolved emission profiles of both SiH and H_β species have been recorded under these conditions and the results were compared to the performance of the cells incorporating these layers.

Fig. 2 presents the time-averaged axial emission profiles resulting from one-electron impact dissociative excitation of SiH_4 towards SiH ($A^2\Delta$), a process with an appearance threshold of 10.5 eV [4], at the pressure of 5 Torr. The shape of the emission profiles reflects the distribution of effective electrons, having energy higher than the process threshold. As one can observe this distribution is strongly affected by the increase of the SiH_4 fraction in the mixture. Namely, for percentages between 0.5% and 1.5% the profiles show a rather sharp maximum of intensity located closer to the RF electrode (~3–4 mm) whereas a further increase of SiH_4 fraction result in a relative enhancement of the production of excited species in the bulk of the plasma and consequently closer to the grounded electrode. Taking into account the fact that in these high pressure conditions the main mechanism through which the electrons gain energy is ohmic heating [5], one can say that the increase of SiH_4 fraction leads to an enhancement of the bulk relative to sheath ohmic heating mechanism. This change can be either attributed to the weakening of the RF field in the sheath, caused by the increase of the density of large SiH_4 molecules, or to the enhancement of the bulk field due to electron attachment to SiH_4 molecules. Whatever the case, the change of the distribution of electrons having enough energy to dissociate SiH_4 will certainly affect the film growth since it will shorten the distance between the growing film surface and the point where film precursors are initially produced. This will result in a modification of the relative flux of species reaching the surface (H, SiH_2, SiH_3, etc), because of the different gas phase reactivity of each species, thus modifying their probability to participate in surface reactions.

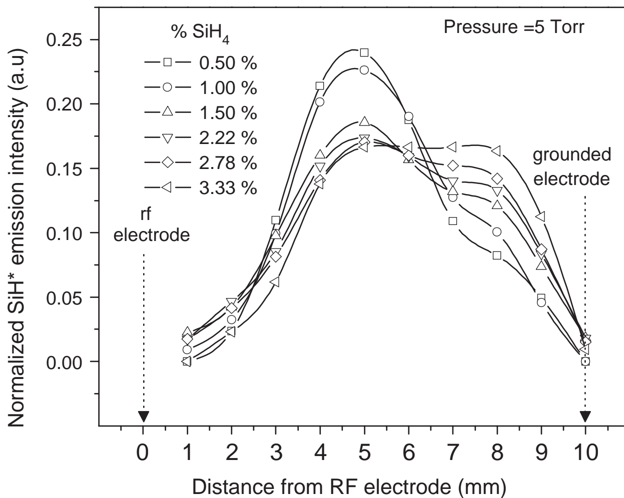

Fig. 2. Spatial distribution of SiH ($A^2\Delta$–$X^2\Pi$) emission intensity in 5 Torr SiH_4/H_2 for six different SiH_4 fractions.

The same effect of silane fraction on the shape of the distribution of the production of species is further demonstrated at the pressure of 10 Torr on another elementary process as well. Thus, Fig. 3 presents the spatial distribution of the normalized emission profiles of the β-Balmer line of atomic hydrogen resulting from one electron dissociative excitation of H_2. The appearance threshold of this process is 17.6 eV, much higher than the SiH* threshold discussed above [6]. The change of the electron heating mechanism in these conditions is more intense compared to the 5 Torr case. Actually, for fractions between 0.5% and 1% the sheath ohmic heating in front of both the powered and grounded electrode sheath leads to the appearance of the two peaks near the electrodes. As expected, electron heating is much more effective near the RF electrode sheath, due to the higher field in this region. However, a further increase of SiH_4 fraction above 1.0% leads to a complete change of the profiles shape that now present only one local maximum of intensity close to the middle of the electrode gap leading to the consequences for the film growth discussed above.

It must be noted here that single point or total emission measurements would fail to reveal this change in the discharge structure. Moreover, this change in the shape of the emission distribution can lead in the recording of false trends when using single point measurements.

Figs. 4(a) and (b) show the initial efficiencies of the solar cells deposited in the p–i–n sequence on ZnO:Al coated glass substrates. The i-layers in these cells were prepared at the conditions used for optical measurements, as described above. In the 5 Torr case (Fig. 4a) the increase of SiH_4 fraction up to 2.25% leads to an almost linear enhancement of the efficiency. However, a further increase result in a drop of the efficiency from 6.3% to 2.9% that is characteristic of the transition from microcrystalline to amorphous silicon growth of the i-layer mainly due to a drop of

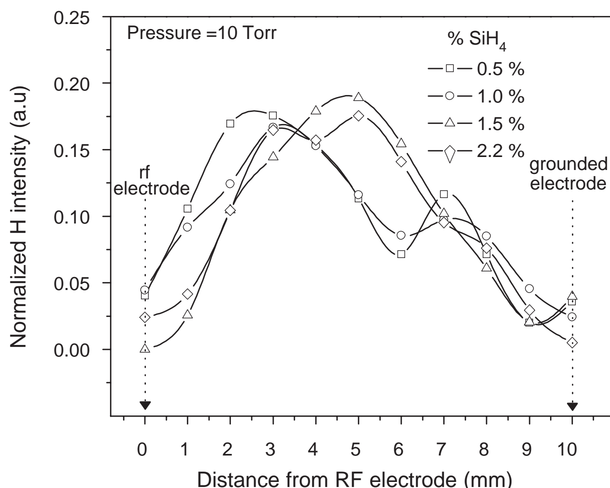

Fig. 3. Spatial distribution of the β-balmer line of atomic hydrogen emission intensity in 10 Torr SiH_4/H_2 for four different SiH_4.

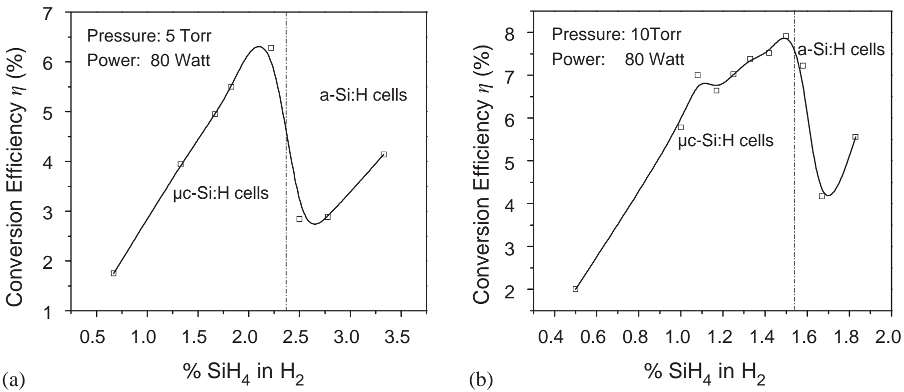

Fig. 4. Cell efficiencies as a function of SiH_4 fraction in the gas mixture at the total pressures of (a) 5 Torr and (b) 10 Torr.

the fill-factor (FF) and the short circuit current (I_{sc}) [7]. In the 10 Torr case (Fig. 4b), the relation between cell efficiency and SiH_4 fraction is the same as for 5 Torr but the transition from microcrystalline to amorphous silicon takes place at a lower silane fraction (i.e., 1.5% compared to 2.25%).

It is clearly observed by comparing the spatially resolved emission to the cell efficiency results that the transition from microcrystalline to amorphous silicon growth can be related to the change of the spatial distribution of radical production. As shown above, in both pressures the change of the emission profile shape occurs at the same range where the cell efficiency drop is observed. The reasons behind this relation are further discussed in the following section.

4. Discussion

The transition from microcrystalline to amorphous silicon growth has been the subject of several studies reported in the literature [8–10]. The reduction of hydrogen flux [8], the increase of ion bombardment [9] and the contribution of highly sticking radicals to the film growth [10] are some of the reasons evoked to explain this transition. In the case of increasing silane fraction discussed here, a reduction of the atomic hydrogen flux due to the reaction of H with SiH_4 may be one reason. Moreover, the production as well as the consumption of highly sticking radicals will be favoured by the increase of SiH_4 percentage. The enhancement or not of the contribution of these radicals to the film growth will then be determined by the distribution of their production in space. This distribution is roughly depicted by the recorded emission profiles because of the very rapid de-excitation of these one electron impact produced species. From this point of view, the profiles presented here can be used to estimate the effect of increasing SiH_4 fraction on the contribution of the species to the film growth.

The probability of a radical to reach the growing surface can be expressed as [11]:

$$P_i(x) = \mathrm{e}^{-v_i\, t} \tag{1}$$

where x is the position between the two electrodes where the specie is generated, v_i is the collision frequency of the radical leading to consumption and t is the time required for the specie to reach the surface if no reactive collisions take place during this trip. Collision frequency can be calculated taking into account secondary gas phase reactions in which the species participate before reaching the surface. In Table 1 is presented the calculated collision frequency for the silylene (SiH_2) radical, taking into account the two most important gas phase reactions of this species [12]:

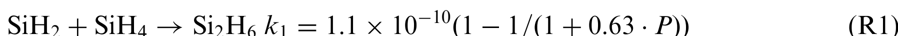

$$SiH_2 + SiH_4 \rightarrow Si_2H_6\; k_1 = 1.1 \times 10^{-10}(1 - 1/(1 + 0.63 \cdot P)) \tag{R1}$$

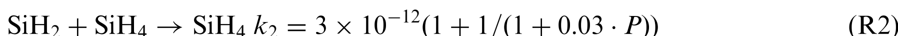

$$SiH_2 + SiH_4 \rightarrow SiH_4\; k_2 = 3 \times 10^{-12}(1 + 1/(1 + 0.03 \cdot P)) \tag{R2}$$

The collision frequency increases with SiH_4 fraction mainly due to R_1 which is much faster than R_2. P in R_1 and R_2 is the total gas pressure expressed in Torr.

The time t required for the SiH_2 radical to reach the surface will depend on the velocity of the species and the distance from the substrate. In order to have an estimation of the SiH_2 velocity one must determine the gas flow regime first. For this, one can use the Pecklet number ($Pe = u \cdot d/D_{SiH_2}$) to determine if diffusion or convection is the main mass transport mechanism and consequently if the gas flow velocity or the thermal (random) velocity will be used for the calculation of time t. For the calculation of Pecklet number at the specific conditions, the total gas flow was used for the determination of velocity u, the interelectrode distance was considered as the characteristic length d, while the Chapman–Enscog theory [13] was used for the calculation of the diffusion coefficient of SiH_2 in the binary mixture. The results of these calculations are summarized in Table 1 where one can observe that Pecklet has values quite smaller than unity, indicating that thermal motion determines the mass transport of SiH_2 radical. Thus, the time t can be calculated

Table 1
Diffusion coefficient (D_{SiH_2}), Pecklet number (Pe), collision frequency for reaction v_i (s^{-1}) and total probability of reaching the substrate for SiH_2 radicals and H atoms at the total pressure of 5 Torr and for different fractions of SiH_4 in the mixture

% SiH_4	D_{SiH_2}	Pe	v_i ($\times 10^5$, s^{-1})	$\Sigma P_{N_{av}}$ (SiH_2)	$\Sigma P_{N_{av}}$ (H)
0.5	250.2	0.00799	5.64	0.00231	0.10006
1	245.6	0.00814	5.69	0.00244	0.09883
1.5	241.3	0.00829	5.75	0.00299	0.09376
2.22	235.6	0.00849	5.82	0.00313	0.09322
2.78	230.7	0.00867	5.88	0.00330	0.09311
3.33	226.3	0.00884	5.93	0.00386	0.09316

according to the relation

$$t = \frac{l}{u_{\mathrm{th}}}, \tag{2}$$

where, l is the distance of the radical from the substrate and $u_{\mathrm{th}} = \sqrt{k_b \cdot T/\pi \cdot m_{\mathrm{SiH_2}}}$ the species thermal velocity. Using the calculated values of v_i and t in Eq. (1) permits the calculation of the probability P of SiH_2 radical to reach the substrate, starting from each point of the interelectrode gap. In Fig. 5 (a) is presented the variation of $P_{\mathrm{SiH_2}}$as a function of the initial position of the radical and as a function of SiH_4 fraction. The increase of the distance from the substrate, placed at $x = 1$, results in a continuous drop of the probability to contribute to the film growth. On the other hand, the increase of % SiH_4 fraction leads to a drop of $P_{\mathrm{SiH_2}}$ if one compares probabilities for the same x mainly due to R_1 favoured by the increase of SiH_4 concentration.

However, these calculations are only valid for a uniform spatial distribution of the generation of the species. As already observed in the emission profiles presented, this is never the case in real discharges where the spatial non-uniformity has to be taken always into account. Therefore, the total number of SiH_2 radicals that will reach the substrate from a specific distance x should be expressed as:

$$N(x)\ \ P_{\mathrm{SiH_2}}(x) = N(x)\mathrm{e}^{-v_i t(x)}, \tag{2a}$$

where, $N(x)$ is the density of SiH_2 radicals at a position x. The value of $N(x)$ is related to the average density of SiH_2 and to the emission intensity distribution as follows:

$$N(x) = N_{\mathrm{av}} \frac{I(x)}{I_{\mathrm{TOT}}}, \tag{3}$$

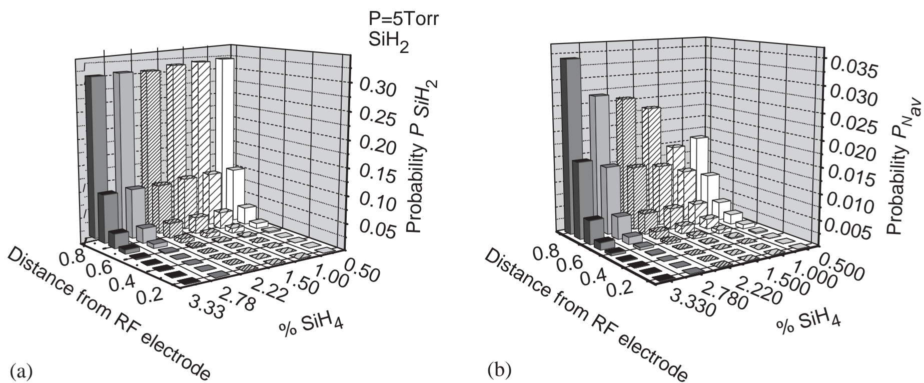

Fig. 5. (a) Probability of SiH_2 radicals to reach the surface as a function of their generation position and the SiH_4 fraction in the gas mixture (uniform generation), and (b) total probability of SiH_2 radicals to reach the surface as a function of their generation position and the % fraction of SiH_4 (non-uniform generation according to the spatially resolved emission profiles of Figs. 2 and 3). Substrate position $x = 1$.

where $I(x)/I_{\mathrm{TOT}}$ is the normalized emission intensity. Substitution of Eq. (3) to Eq. (2a) result in an expression of the form:

$$N(x)\,P_{\mathrm{SiH}_2}(x) = N_{\mathrm{av}}\frac{I(x)}{I_{\mathrm{TOT}}}\,\mathrm{e}^{-v_i t(x)} = N_{\mathrm{av}}P_{N_{\mathrm{av}}}(x). \tag{4}$$

The function $P_{N_{\mathrm{av}}}(x)$ on the right-hand side of Eq. (4) holds all the information concerning the effect of spatial non-uniformity on the probability of SiH_2 radicals to reach the surface. This term multiplied by the average density (N_{av}) gives the probability of SiH_2 radicals to reach the surface starting from point x. Thus, in Fig. 5(b) is presented the variation of $P_{N_{\mathrm{av}}}$as a function of the position in the discharge and as a function of the SiH_4 fraction in the gas mixture. This time the effect of SiH_4 fraction is far more important than in the case of uniform production revealing the importance of the spatial distribution of radical production in the discharge. Namely, the increase of SiH_4 fraction significantly increases the probability of SiH_2 radicals, originating not further than 4 mm away from the surface, to contribute to the film growth. The radicals generated in those 4 mm give the observed increase of their probability of contribution despite the increase of their consumption with silane fraction. This is clearly a result of the change of the spatial distribution of radicals that enhances the production of species very close to the surface as observed in the emission measurements.

Moreover, the total probability of SiH_2 radicals to reach the growing film surface was calculated by integrating $P_{N_{\mathrm{av}}}$ over the interelectrode space and the results show an increase of $P_{N_{\mathrm{av}}}$ with % SiH_4 fraction (Table 1).

The analysis presented so far revealed the specific importance of the spatial distribution of radical generation in the discharge on their probability to reach the growing film surface for SiH_2, which is a radical with rather high reactivity in the gas phase. It is clear from this discussion that species with lower gas phase reactivity will be less affected by the change of the shape of the distribution. Indeed, a similar analysis was also performed for H atoms that have much lower gas phase reactivity and the calculated total probability of these species to reach the surface is included in Table 1. It is observed that the increase of SiH_4 fraction decreases $P_{N_{\mathrm{av}}}$ for H atoms. This is due to the fact that the probability of the much less reactive H atoms is almost unaffected by the change in the shape of their generation profiles, because in every case H atoms have a good chance to reach the surface even if they originate much further than 4 mm away from it. However, their total probability is still affected by the increase of the collision frequency due to the increase of silane density.

The enhanced contribution of high sticking coefficient radicals (like SiH_2) to the film growth, due to the enhancement of their production closer to the surface, combined to the drop of H atom probability with % SiH_4 fraction can probably explain the observed transition from microcrystalline to amorphous silicon growth and the correlation of this transition to the change of shape the emission profiles. Spatially resolved emission spectroscopy has proved to be a sensitive diagnostic tool that, at least in these conditions, can be used for predicting the microcrystalline to amorphous growth transition.

5. Conclusions

Spatially resolved optical emission spectroscopy was evaluated as a diagnostic tool for the prediction of plasma conditions that lead to growth of μc-Si:H films near the transition to amorphous silicon growth.

The transition from microcrystalline to amorphous silicon growth was achieved by increasing the fraction of SiH_4 in the gas mixture and was identified through the performance of the solar cells prepared at these conditions. The shape of the emission profiles of SiH^* and β-balmer line of atomic hydrogen was found to change drastically for SiH_4 fractions around the transition leading to an increase of radical production closer to the deposition surface. This change of the shape of the emission intensity distribution was attributed to the change of the electron heating mechanism from sheath to bulk ohmic heating caused by the increase in silane density.

The effect of the observed change of the spatial profiles on the contribution of various radicals to the film growth was discussed by evaluating their probabilities to reach the growing film surface. The results show that the production of species closer to the substrate enhances the contribution of highly sticking radicals like SiH_2 to the film growth, despite the increase of its consumption due to the increase of silane density. The change of the shape of production has a less significant effect on species with lower gas phase reactivity like H atoms, the probability of which to reach the surface is still decreased because of the increase of the collision frequency with silane. Both these effects can serve as an explanation for the transition from microcrystalline to amorphous silicon growth and also for the relation between the shape of the emission profiles and the transition. In any case the observed change of the shapes must be also evaluated against the large differences in the calculated probabilities between uniform and non-uniform production. These differences point out the systematic flaw of single point or overall emission intensity measurements and the necessity for spatially resolved diagnostics.

Acknowledgements

This work was performed in the framework of the "DOIT" (ENK6-CT-2000-00321) project funded by the Commission of the European Union DG XII.

References

[1] J. Meier, R. Flückiger, H. Keppner, A. Shah, Appl. Phys. Lett. 65 (1994) 860–862.
[2] T. Roschek, T. Repmann, J. Müller, B. Rech, H. Wagner, J. Vac. Sci. Technol. A 20 (2) (2002) 492–498.
[3] S. Suzuki, M. Kondo, A. Matsuda, Sol. Energy Mater. Sol. Cells 62 (2000) 489–495.
[4] S. Tsurubuchi, K. Motohashi, S. Matsuoka, T. Arikawa, Chem. Phys. 161 (1992) 493–500.
[5] M. Surendra, D.B. Graves, IEEE Trans. Plasma Sci. 19 (1991) 144–157.
[6] G.A. Khayrallah, Phys. Rev. A 13 (1976) 1989–2003.
[7] O. Vetterl, F. Finger, R. Carius, P. Hapke, L. Houben, O. Kluth, A. Lambertz, A. Muck, B. Rech, H. Wagner, Sol. Energy Mater. Sol. Cells 62 (2000) 97–108.

[8] Y. Yang, M. Katiyar, G.F. Feng, N. Maley, J.R. Abelson, Appl. Phys. Lett. 65 (1994) 1769–1771.
[9] M. Kondo, M. Fukawa, L. Guo, A. Matsuda, J. Non-Cryst. Solids 266–269 (2000) 84–89.
[10] E. Amanatides, D. Mataras, D.E. Rapakoulias, Thin Solid Films 383 (2001) 15–18.
[11] F. Reif, Fundamentals of Statistical and Thermal Physics, McGraw-Hill, New York, 1965.
[12] J. Perrin, O. Leroy, M.C. Bordage, Contrib. Plasma Phys. 36 (1996) 3–49.
[13] R.B. Bird, W.E. Stewart, E.N. Lightfoot, Transport Phenomena, Wiley, New York, 1960.